High-pressure behavior of CsC_8 graphite intercalation compound: Lattice structures and phase-transition mechanism

N. Rey,[1] P. Toulemonde,[1,2] D. Machon,[1] L. Duclaux,[3] S. Le Floch,[1] V. Pischedda,[1] J. P. Itié,[4] A.-M. Flank,[4] P. Lagarde,[4] W. A. Crichton,[5] M. Mezouar,[5] Th. Strässle,[6] D. Sheptyakov,[6] G. Montagnac,[7] and A. San-Miguel[1,*]

[1]*Laboratoire de Physique de la Matière Condensée et Nanostructures, CNRS, UMR 5586, Université Lyon 1, F-69622 Villeurbanne, France*

[2]*Département MCMF, Institut Néel, CNRS and Université Joseph Fourier, 25 Avenue des Martyrs, Boîte Postale 166, F-38042 Grenoble Cedex 9, France*

[3]*Laboratoire de Chimie Moléculaire et Environnement, Université de Savoie-ESIGEC, Campus Scientifique de Savoie-Technolac, Le Bourget du Lac Cedex, France*

[4]*Synchrotron-SOLEIL, CNRS-UR1, Boîte Postale 48, 91192 Gif-sur-Yvette Cedex, France*

[5]*European Synchrotron Radiation Facility, rue 6 Jules Horowitz, Boîte Postale 220, 38043 Grenoble Cedex 09, France*

[6]*Laboratory for Neutron Scattering, ETH Zurich & Paul Scherrer Institut, CH-5232 Villigen PSI, Switzerland*

[7]*Laboratoire de Sciences de la Terre, UMR 5570, CNRS-ENSL-UCBL, 46 Allée d'Italie, F-69364 Lyon Cedex 07, France*

(Received 19 October 2007; revised manuscript received 23 January 2008; published 27 March 2008)

The high-pressure phase diagram of CsC_8 graphite intercalation compound has been investigated at ambient temperature up to 32 GPa. Combining x-ray and neutron diffraction and Raman and x-ray absorption spectroscopies, we report that CsC_8 when pressurized undergoes phase transitions around 2.0, 4.8, and 8 GPa. Possible candidate lattice structures and the transition mechanism involved are proposed. We show that the observed transitions involve structural rearrangements in the Cs subnetwork, while the distance between the graphitic layers is continuously reduced at least up to 8.9 GPa. Around 8 GPa, important modifications of signatures of the electronic structure measured by Raman and x-ray absorption spectroscopies evidence the onset of a transition which could imply a change of stage. Finally, we also provide the *c*-axis compressibility of CsC_8 between 0 and 8.9 GPa.

DOI: 10.1103/PhysRevB.77.125433 PACS number(s): 81.05.Uw, 64.70.K−, 61.50.Ks, 71.20.Tx

I. INTRODUCTION

Graphite intercalation compounds (GICs), well-known basic two-dimensional systems, have been extensively studied as template layered materials, allowing the intercalation of numerous different chemical species ($\geqslant 100$).[1] A recent renew of interest on GICs has been motivated by the discovery of the highest superconducting critical temperature T_c of this family of materials in CaC_6 (11.5 K) and YbC_6 (6.5 K),[2,3] leading to subsequent experimental[4–9] and theoretical[10–15] efforts.

Pressure is a crucial thermodynamic parameter in the understanding of electronic and structural properties of these low dimensional guest-host systems. Pressure effects include, in particular, the enhancement of the host-guest interactions. In addition, under high-pressure (HP) and high temperature conditions, GICs can constitute precursors for the formation of new carbon intercalated materials such as carbon clathrates,[16] which could show promising superconductivity[17] and mechanical[18] properties.

In GICs, several structural modifications associated with the layered topology such as staging, in-plane decoration, or stacking schemes are observed. One of the most remarkable structural features is the staging phenomenon occurring at long-range order.[1] Staging refers to the one-dimensional periodic alternation of filled and empty graphitic galleries. Stage *n* is defined as the structure in which intercalates are accommodated regularly in every *n*th graphite layer. Thus, for stage 1, all the graphitic galleries are periodically occupied by the intercalate layers. The repeat distance I_c is defined as the distance along the *c* axis between two successive intercalated layers. Important structural features are distinguished according to the value of the stage index *n*. Another important feature encountered in GIC structures is decoration. It refers to the crystalline arrangement of the intercalate in the two-dimensional plane. Two different decorations of intercalated layers commensurate to the graphite lattice for the stage-1 donor compounds have been observed: a hexagonal 2×2 superlattice (Rb, Cs, and K) and a hexagonal $\sqrt{3}\times\sqrt{3}$ superlattice (Li, Ca, Yb, and others). In higher stage compounds, the metal layer arrangement can lead to an incommensurate modulation with respect to the graphite layers or can be even similar to a *liquid like* behavior.[19,20]

Among the donor compounds, the family of K GICs has been used as model for the description of pressure-induced transitions. The data from different studies were limited to relatively low values of pressure (<3 GPa). In the stage-1 KC_8, staging transitions occurred with the presence of a stage 2 and a fractional stage 3/2 in the 0–3.0 GPa range.[21] Bloch *et al.* observed a $\sqrt{3}\times\sqrt{3}$ superlattice in the same pressure range.[22] These structural changes in the decoration and in the staging are accompanied with an anomaly in the resistivity at 1.5 GPa.[23] No staging transitions were found in CsC_8 and RbC_8 up to 1 GPa,[24] although there were observed pressure-induced anomalies in the resistivity of these two compounds at 2.0 GPa.[23] In the stage-1 CaC_6, pressure induces the enhancement of superconductivity, and near 8 GPa, a structural instability was found when the critical temperature T_c suddenly drops.[25] Similar behavior of T_c in YbC_6 is observed at 1.8 GPa.[26]

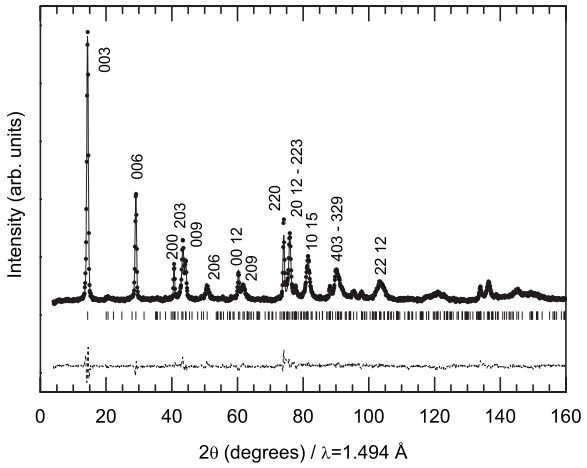

FIG. 1. Ambient pressure and temperature neutron powder diffraction pattern of CsC_8 fitted within a Rietveld refinement. The pattern was collected in a vanadium container.

For "diluted" intercalation, i.e., $n \geqslant 2$, staging transitions $n \rightarrow n+1$ or $n+2$ were observed at moderate pressures of 0.5–1.0 GPa. First, staging transition from stage 2 to stage 3 was evidenced in KC_{24} by Clarke *et al.*[27] This work has been extended to higher stage K GIC and to high-stage Rb and Cs GICs by Wada.[24]

CsC_8 is a good candidate to investigate the size effect on the guest-host interaction with pressure and to give new insight into the high-pressure properties and stability of this important class of materials. The total lack of information for $P > 2$ GPa prompted us to examine this compound at a higher pressure. We have hereby explored the high-pressure evolution up to 32 GPa of CsC_8. Information on the Cs subnetwork has been obtained using x-ray diffraction thanks to the high Z of the guest species. On the other side, neutron diffraction appears as more sensitive to the carbon subnetwork. Finally, local probes that constitute Raman and x-ray absorption spectroscopies are an excellent complement of the long-range order technique, that is, diffraction. This multitechnique approach is a key point for the understanding of the high-pressure behavior of this highly reactive and complex ordered material. In particular, we have investigated the pressure-induced effects such as charge transfer between the guest and host species, the structural modifications in the Cs, and the graphitic subnetworks.

II. EXPERIMENTAL RESULTS

A. Synthesis route and structural characterization

CsC_8 powder samples were synthesized from a high purity stoichiometric mixture of powder graphite (Aldrich, <20 μm) and Cs metal melt (Alfa Aesar, 99.98%) in an argon filled glovebox.[28] A 48 h annealing of the sample in a vacuum sealed glass ampoule allowed to prepare the "brown (reddish)" compound. Figure 1 shows the neutron powder diffraction pattern of our CsC_8 powder measured at ambient conditions together with the residual of the Rietveld refinement using the FULLPROF software.[29] Our structural model includes an anisotropic size broadening effect. A better quality refinement was found when the Cs atoms are in the $3d$ Wyckoff position ($\chi^2=2.73$) rather than in the $3b$ position ($\chi^2=3.74$), as Guérard *et al.* suggested.[30] A $3b$ position would imply an $\alpha\alpha\alpha$ stacking sequence for the Cs atoms, whereas the stacking sequence for this compound is supposed to be $\alpha\beta\gamma$ which can be reproduced with the $3d$ setting. The structural parameters obtained from the refined model are presented in Table I.

TABLE I. Structural parameters of the hexagonal structure of CsC_8 at ambient conditions obtained from a Rietveld refinement. The corresponding stacking is $A\alpha A\beta A\gamma$. Thus, the c-axis lattice parameter corresponds to $3I_c$.

Space group, No.	$P6_222$, 180
Lattice constants (Å)	$a=4.9601$, $c=17.847$
Repeat distance (Å)	$I_c=c/3=5.949$
Atoms	**Wyckoff positions**
C	$12k$ (1/6,1/3,1/3)
C	$6i$ (5/6,2/3,0)
C	$6i$ (2/3,1/3,0)
Cs	$3d$ (1/2,0,1/2)

B. High-pressure diffraction

1. Experimental procedure

We have collected both high-pressure x-ray and neutron powder diffraction data up to 14 and 8.9 GPa, respectively. Angle-dispersive x-ray diffraction (XRD) at the ID27 beamline of the European Synchrotron Radiation Facility (ESRF) was performed using a monochromatic radiation ($\lambda = 0.26472$ Å) and a diamond anvil cell (DAC). The powder sample was loaded inside a 150 μm hole of a steel gasket with heavy mineral oil as pressure transmitting medium (PTM) and placed between the anvils of the DAC with diamond culets of 600 μm. Due to the high reactivity of the sample in the presence of oxygen and humidity, all loadings of the DAC were made inside an argon filled glovebox. The heavy mineral oil PTM ensures a further protection of the sample. A charge-coupled device (CCD) detector was used to collect the high-pressure diffraction images. Calibration of the sample-detector distance and the tilt angle were done with a Si-diamond powder standard. The two-dimensional image files were azimuthally integrated with the FIT2D software yielding one-dimensional intensity versus 2θ diffractograms.[31] The pressure was determined with the ruby fluorescence method.[32] *In situ* angle-dispersive neutron powder diffraction (NPD) experiments were carried out at the HRPT diffractometer[33] located at the Swiss spalliation source (SINQ) using a VX5 Paris-Edinburgh Press[34] in a radial configuration. In this geometry, the incident beam (monochromatic radiation of $\lambda = 1.494$ Å) and the diffracted beam pass through the TiZr gasket in the equatorial plane of the anvils. Neutron absorbing cubic boron nitride (BN) anvils and null-scattering TiZr alloy gaskets were used in order to omit any signal from the pressure cell. Full details of the

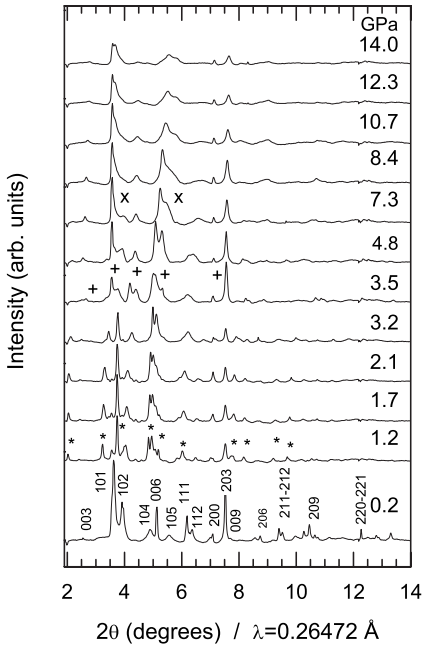

FIG. 2. Selected x-ray diffraction patterns of the CsC_8 compound as a function of pressure. Pressure in GPa is given at the right side of each curve. The first pressure pattern corresponds to the hexagonal structure (CsC_8 I). The sample was confined in oil as the pressure transmitting medium. Intensity was normalized for all patterns to the same counting time. Star (⋆), plus (+), and cross (×) symbols show the appearance of new Bragg peaks corresponding to CsC8 II, CsC8 III, and CsC8 IV phases, respectively (see Table IV).

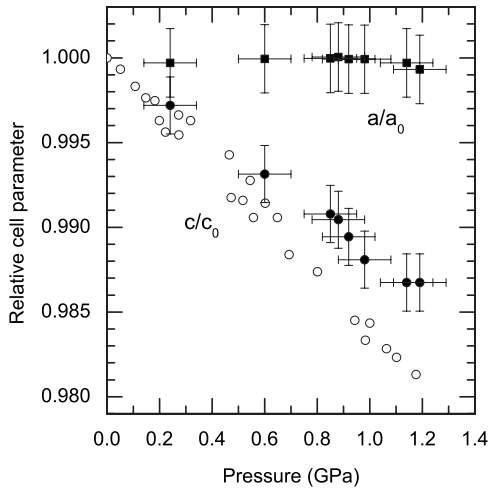

FIG. 3. Compressibility of the hexagonal CsC_8 lattice parameters (solid symbols) derived from our x-ray diffraction experiment and of the c axis reported by Wada (open symbols show two sets of data) (Ref. 24).

experimental setup are described in Ref. 35. The assembly of the gasket and the loading of the press were completed inside a helium filled glovebox. Dried NaCl was used as pressure marker.

2. X-ray diffraction results

High-pressure XRD of CsC_8 was performed up to 14.0 GPa. A sequence of selected diffraction patterns is displayed in Fig. 2. The first sample pattern inside the cell assembly recorded at 0.2 GPa matches the hexagonal ambient structure. No traces of oxide or hydroxide have been found. Inhomogeneous grain size distribution, preferential orientation effects, and the identified stacking faults render a Rietveld refinement or even a Le Bail refinement extremely complex. The very low intensity observed for the (003) and the (009) peaks makes their positions difficult to point out. Only the (006) line provides us a direct reliable information about the c-axis compressibility. Gradual transformation under increasing pressure is the most eye-catching feature as well as the overall decrease of intensity of the diffraction patterns. At 1.2 GPa, we observe the coexistence of the hexagonal phase and a second phase. This second phase is clearly established at 2.0 GPa. At 3.5 GPa, changes in the diffraction pattern evidence again a phase transformation. Furthermore, we notice that the number of peaks of this last high-pressure phase is lower than in the preceding phases, which could be associated with a higher cell symmetry or to a smaller lattice. As the pressure increases from 7.3 to 14 GPa, the diffraction line broadening becomes more and more pronounced, and the profile becomes highly asymmetric.

Let us turn to the compressibility of the starting hexagonal phase at low pressures. Figure 3 shows the lattice parameter evolution with pressure, as obtained from our XRD experiment. The compressibility along the c axis was found to be slightly lower than the one measured by Wada.[24] The difference must be moderated by considering the error bars and the use of different starting graphite samples for the two experiments. Wada used single crystal graphite, while we used powder graphite. We deduce a linear c-axis compressibility κ_c of 1.079×10^{-2} GPa^{-1} corresponding to a linear bulk modulus B_c of 93 GPa (see Table II). The a lattice parameter was found to be very rigid in this pressure range. We estimated the bulk modulus B_v=94 GPa, close to the linear interplane bulk modulus.

Different attempts to determine the crystal structures of the high-pressure phases appearing above 1.2 and 3.5 GPa were carried out. The presence of a diffraction line at very low angle ~2° corresponding to a d spacing of 7.69 Å prompted us to look for a larger crystalline cell assuming a new stacking. We propose the space group $C222$ as a possible candidate for the first HP phase. This choice corresponds to a space group search procedure with the CRYSFYRE SUITE[36] and CHECKCELL[37] softwares. Among the possible space groups obtained, $C222$ reproduced best the experimental data. The corresponding orthorhombic lattice is described in terms of a supercell with parameters fitted within a Le Bail refinement (Table III). The lattice parameters of the second HP phase, observed between 3.5 and 8.0 GPa, were found to be very close to the orthorhombic cell defined in RbC_8 (Ref. 38) and in CsC_4,[39] a superdense metastable phase of Cs GICs. We used the same space group $Fddd$ and Wyckoff positions as RbC_8 for the refinement model. This supposes a change of the stacking from $\alpha\beta\gamma$ to $\alpha\beta\gamma\delta$ with a corresponding $I_c=c/4=5.72$ Å (a=4.39 Å, b=9.20 Å, and c =22.87 Å) instead of 5.945 Å at ambient pressure (Table III). Figure 4 shows the Le Bail refinement and residuals for

TABLE II. Axial compressibility and bulk modulus of CsC_8 in comparison with graphite. Incertitudes for our values are 10%.

Techniques	B_c (GPa)	B_c'	B_v (GPa)	B_v'	P range
XRD (this work)[a]	93	0	94	0	0–1.1 GPa
INS[b]	58				Ambient
XRD[c]	64				0–1.1 GPa
NPD (this work)	72	8	70	6	0–8.9 GPa
Graphite[d]	36.4				Ambient

[a]Linear fit.
[b]Inelastic neutron scattering (INS) from Ref. 56.
[c]Reference 24.
[d]X-ray inelastic scattering from Ref. 57.

the two HP phases using the GSAS analysis software.[40] The two refinements are not completely satisfying: in the 4.8 GPa refinement, essentially, broadening is not taken into account as we can see, and in the 2.0 GPa refinement, the position of the peak located around 2° is not well reproduced. In order to check the validity of our proposed lattices and to go deeper into the structural determination, i.e., to determine the atomic positions, better complementary and/or quality data are needed.

3. Neutron powder diffraction results

We consider now the neutron diffraction data. In contrast to the x-ray case, where diffraction is dominated by the scattering cross section of Cs, neutron diffraction is expected to provide a better information for the carbon subnetwork because of the better balance between the scattering cross sections of carbon (σ_{coh}=5.551 barn) and Cs (σ_{coh} =3.690 barn). Due to the characteristics of the HP device, the maximal pressure was limited to 8.9 GPa. Three different experiments have been done: sample with NaCl (experiment 1), sample with mineral oil (experiment 2), and sample without any PTM and hence no pressure calibrant (experiment 3). The reversibility of the high-pressure transformation was obtained in all the three cases after complete pressure release from 8.9 GPa, as shown in Fig. 5 for the first experiment. In the second experiment, the important incoherent background signal from the oil PTM did not allow us to collect good quality data when increasing pressure. The pressure evolution of the c and a axes of CsC_8 from the first experiment is displayed in Fig. 6. By using the pressure-force calibration curve of the first experiment as the pressure scale of the third experiment, its analysis leads to the same pressure dependence of the lattice parameters than for the first one. The compressibility of CsC_8 in the basal direction matches the compressibility of the graphite a axis, whereas the presence of intercalated Cs atoms produces a stiffening of the c axis. In spite of the poor signal-to-noise ratio, appreciable changes in the intensity ratio between the (003) and (006) lines (Fig. 7) and in the broadening of the lines of the neutron data tend to support the observed transitions by XRD corresponding to the I→II transition around 1 GPa and maybe III→IV transition around 8 GPa.

Contrarily to the XRD experiments, no evident sign of phase transformation was found between 1.9 and 8.9 GPa. We only noticed the presence of two very low-intensity peaks, around 11° (7.8 Å) and 22°–24° (3.6–3.9 Å) (see stars in Fig. 5), when increasing pressure and which remain detectable after releasing the pressure to zero. The origin of these peaks is not clearly understood but no significant shift with pressure associated with these peaks is observed. Con-

TABLE III. Structural parameters of the possible candidate phases of CsC_8 appearing at 2–3 and 4.8 GPa. The quality of the Le Bail fits only allows to propose these structures as indicative of the complexity of the high-pressure structures.

	2.0 GPa	4.8 GPa
Space group, No.	*C222*, 21	*Fddd*, 70
Lattice constants (Å)	$\alpha=\beta=\gamma=90°$	
a	5.24	4.39
b	6.02	9.20
c	56.75	22.87

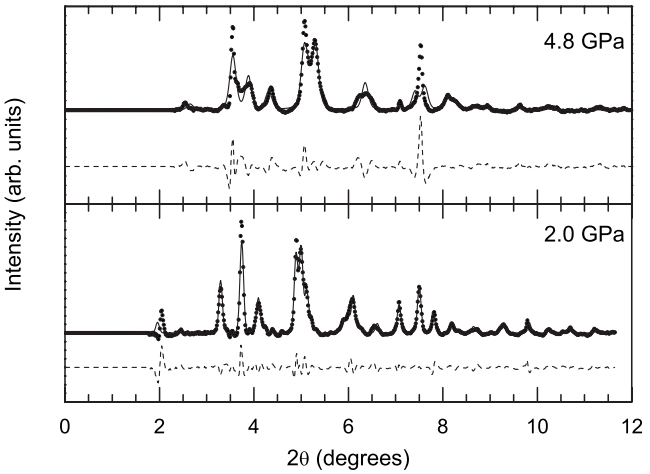

FIG. 4. Le Bail refinements of the x-ray diffraction data for the high-pressure phases of CsC_8 at 2.0 GPa (bottom) and 4.8 GPa (top) corresponding to structural models shown in Table III.

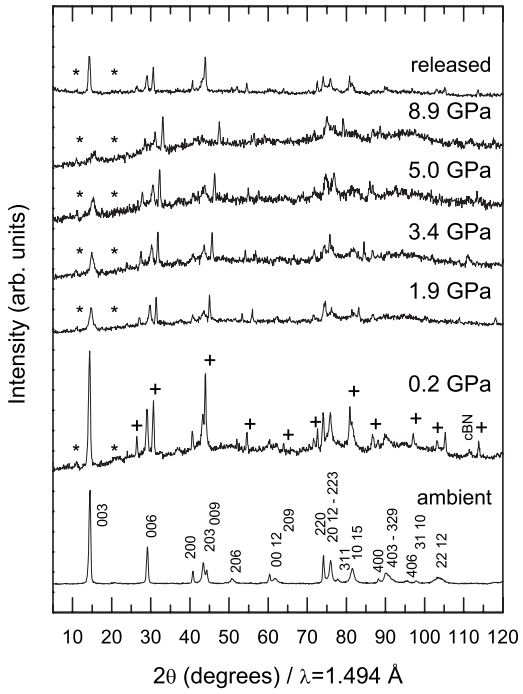

FIG. 5. Neutron powder diffraction patterns of CsC_8 as a function of pressure with NaCl (+) as the pressure transmitting medium and pressure marker. The two stars (⋆) indicate additional peaks (see text). The ambient diffraction pattern was taken in a vanadium container. The released pressure diffraction pattern was recorded in the press after the HP cycle.

sequently, they cannot correspond to the (00ℓ) lines of stage 3/2, as it was previously reported in KC_8.[21,42] In addition, the extrapolated lattice parameters of the superdense CsC_4 phase (using the *c*- and *a*-axis compressibilities of Fig. 6) observed by Nalimova *et al.* around 0.5–1 GPa (Ref. 39) cannot either explain these very weak peaks. Consequently, they could most probably result either from the presence of a

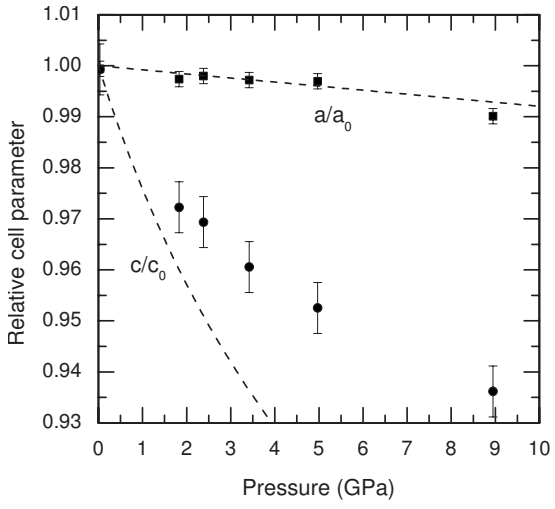

FIG. 6. Evolution of the lattice parameters of CsC_8 (filled symbols) from NPD as a function of pressure compared to the graphite ones (dashed lines) from Ref. 41. The errors bars are provided from the Rietveld refinements.

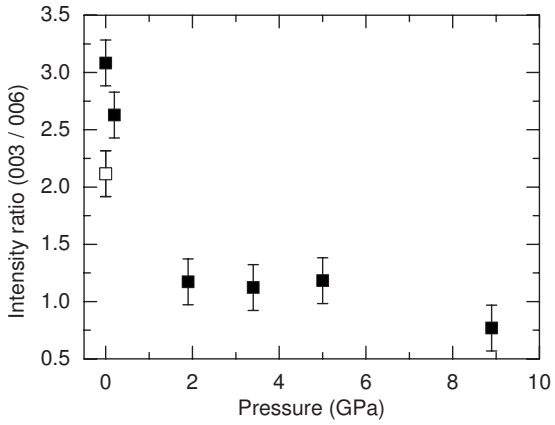

FIG. 7. Evolution of the relative intensity of the (003) and (006) diffraction lines with pressure (solid symbols). Open symbol is for the decompression at zero pressure.

minority phase corresponding to an impurity or from the HP environment.

Combining x-ray and neutron diffraction appears then to be relevant to understand the behavior of CsC_8 under pressure. The observed differences between XRD and NPD results can be attributed to two facts. First, XRD is essentially sensitive to the Cs layer order, while NPD patterns are dominated by the C atom contribution. Secondly, the scattering geometries are different for the NPD (radial geometry) and XRD (axial geometry) experiments. It seems that due to the preferential orientation effect occurring with pressure in this lamellar compound, as it was observed for graphite,[43] the radial geometry is better adapted to follow the (00ℓ) lines. At least two clear transitions have been evidenced at 2.0 and 4.8 GPa by XRD associated with changes in the decoration of the Cs layer and in the stacking. On the other side, the NPD data show us that such transitions do not imply a structural change in the graphitic (host) subnetwork (Fig. 5). We observe a stiffening of the *c* axis in CsC_8 in comparison with graphite. Hence, neutrons reveal that under high pressure, the initial average structure of CsC_8 initial phase is not strongly modified.

C. Raman spectroscopy

The Raman spectra were collected with a LabRam HR800 spectrometer from Jobin-Yvon equipped with a CCD detector in the backscattering geometry. Spectra were excited using 632.8 nm radiation from a He-Ne air-cooled laser, Spectra Physics™. Low power radiation from the laser source (a few milliwatts) was tuned to avoid deintercalation effects caused by the local heating.[44,45] The laser beam was focused into the DAC through a Mitutoyo 50× objective down to a laser spot size of approximately 2 μm. The DAC was loaded inside an argon filled glovebox to prevent the contamination of the highly sensitive sample to oxygen or humidity. Stainless steel gaskets of 30 μm thickness were drilled to 135 μm hole diameter. Heavy mineral oil was used as a PTM in the pressure chamber. Ruby chips served for pressure calibration.

The CsC_8 Raman spectrum at ambient pressure is shown in Fig. 8. Characteristic features are a high-frequency broad

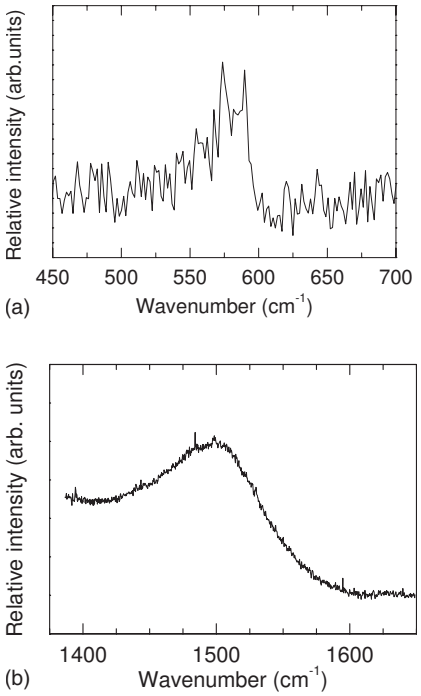

FIG. 8. (a) Low-frequency and (b) high-frequency Raman signals of CsC_8 at ambient pressure and room temperature with a 632.8 nm laser excitation.

structure (at approximately 1500 cm^{-1}) and a low-frequency structure (near 560 cm^{-1}) in agreement with previous studies.[44,45] Intercalation of donor species such as the alkali leads to a metallic behavior instead of the semimetallic (graphite) character. This metallic character is more pronounced for rich alkali/C atom compositions, typically for stage-1 compounds as in our case, making the detection of the Raman scattering signal difficult. Two first-order active Raman modes can be observed for pristine graphite, at 42 and 1582 cm^{-1}. In GICs, the guest intercalate alkali layers act like a perturbation on the graphite modes, thus leading to a shift in frequency[46] and turning on new active Raman modes. The striking high-frequency broad asymmetric line is interpreted as a Breit-Wigner-Fano (BWF) resonance.[47] This BWF line shape arises from an interaction of an electronic continuum with in-plane carbon-layer vibration corresponding to the Γ-point mode of pristine graphite. However, the origin of the singular structure in the vicinity of 560 cm^{-1} which is, in fact, a triplet[48] rather than a doublet still remains unclear. This special feature was ascribed to a zone folding of M_{1g} modes into the Γ point for the (2×2) superlattice corresponding to the MC_8 formula,[45] whereas the triplet was well accounted by disorder-induced scattering.[48]

Figure 9 shows the behavior of the low-frequency domain from 0.1 to 3.2 GPa. The first spectrum collected in the DAC is in perfect agreement with the signal at ambient pressure reported in Fig. 8(a). The signal-to-noise ratio becomes of better quality as the pressure increases and we observe a better resolved triplet at 1.4 GPa. Then, the triplet gradually disappears above 1.4 GPa and cannot be detected beyond 3.2 GPa. Within our accuracy, no significant shift of the triplet frequencies is observed.

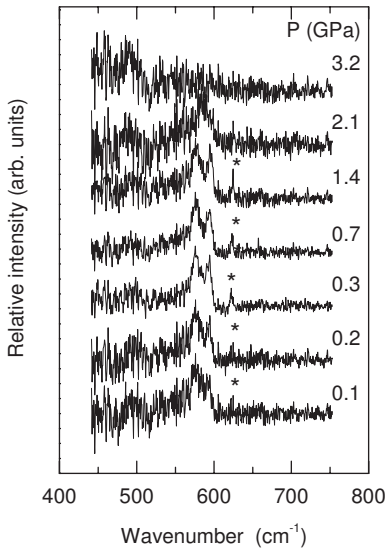

FIG. 9. Low-frequency Raman spectra of CsC_8 as a function of pressure. The star indicates the weak component consistent with the triplet observed by Caswell and Solin (Ref. 48).

During the compression study, several changes of the high-frequency mode have been observed. Selected high-frequency Raman spectra of the CsC_8 compound taken at different pressures are presented in Fig. 10, showing the pronounced asymmetric broad shape associated with the BWF resonance. In the low pressure region, 1.4–2.1 GPa, the complete disappearance of the low-frequency triplet is ac-

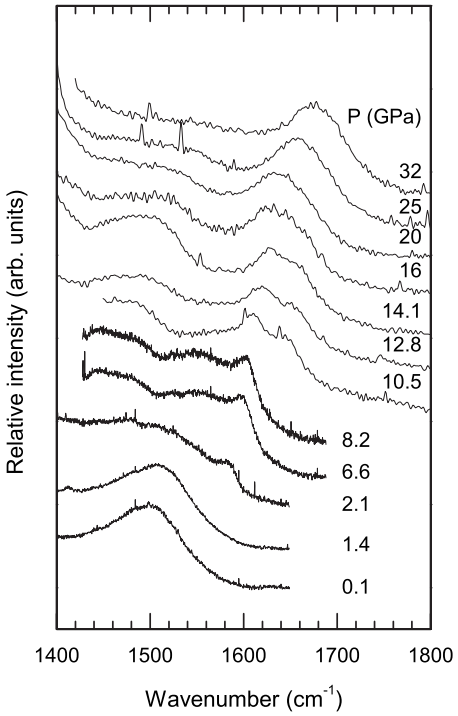

FIG. 10. High-pressure evolution of the high-frequency Raman spectra of CsC_8 at room temperature. From 0 to 8.2 GPa, Raman spectra were collected using a 1800-line grating and a 600-line grating was used from 10.5 to 32.0 GPa. The background is strengthened with the Raman contribution of the oil.

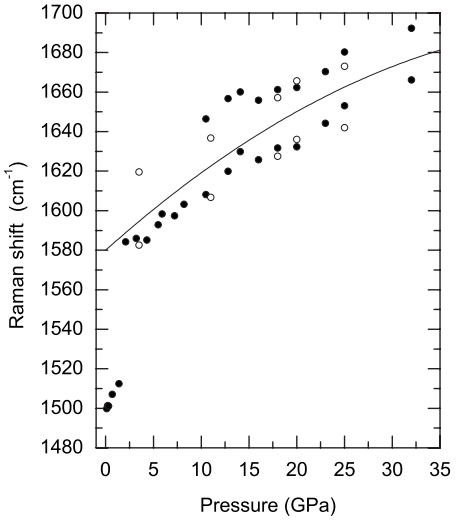

FIG. 11. High-frequency Raman region peak positions of CsC_8 versus pressure. The continuous line indicates the evolution of the E_{2g} graphite mode with pressure from Ref. 49. Filled circles represent the compression, whereas open circles show the decompression of the sample.

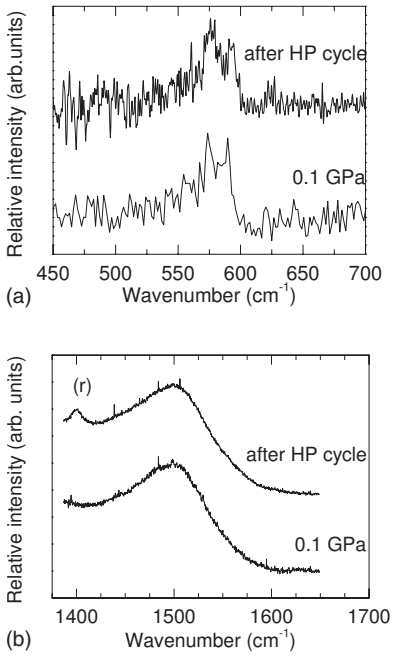

FIG. 12. Comparison of the (a) low-frequency and (b) high-frequency Raman spectrum of CsC_8 between the first pressure point at 0.1 GPa in the DAC and after the HP cycle to 8.2 GPa. Fluorescence of ruby is indicated by the (r) label.

companied by a large shift of the BWF resonance from around 1500 to 1590 cm^{-1} (Fig. 11). At 10.5 GPa, another peak appears close to the first one but slightly upshifted, resulting in a doublet. Above 16 GPa and up to 32 GPa, it is extremely difficult to dissociate the two peaks, due to their large broadening.

Upshifted Raman frequencies from the graphite mode (1582 cm^{-1}), visible above 10.5 GPa (Fig. 10), have been also observed in the case of diluted Cs GICs. At ambient pressure, the stage-2 compound CsC_{24} exhibits a Raman peak at 1598 cm^{-1}.[44,45] In the higher diluted compound such as the CsC_{36} stage 3, a doublet (1604–1579 cm^{-1}) is observed at ambient pressure.[44,45] The lower frequency of this doublet is related to interior graphitic layers, whereas the upper frequency is ascribed to the bounding graphitic layers. The high-frequency doublet is systematically present for $n>2$ when the screening of the interior graphite layer by the bounding layer is not efficient anymore. The pressure behavior of the E_{2g} graphite mode of graphite from Ref. 49 is also shown in Fig. 11. We remark that the peak appearing in the CsC_8 spectrum at 2.1 GPa around 1585 cm^{-1} corresponds with the evolution of the graphite E_{2g} peak and therefore could be associated with the interior graphitic layer mode observed in stage n with $n>2$. Consequently, the higher frequency of the doublet could be associated with the bounding layer mode. When the pressure is released from 32 to 3.5 GPa, a reversible transformation accompanied with a hysteresis is observed (Fig. 11). Due to technical reasons, we were not able to collect a Raman spectra at ambient pressure in the DAC.

The initial Raman spectrum is recovered when the pressure is totally released from a maximum pressure of 8.2 GPa (Fig. 12), indicating the reversible backtransformation to the ambient phase of CsC_8, as previously observed in our NPD experiments reported here. Thus, assuming a deintercalation process involving diffusion of the alkali atoms outside the graphitic host above 2 GPa is incompatible with the observation of the CsC_8 low- and high-frequency features after the complete decompression, i.e., the reversibility of the Raman signal (Fig. 12).

D. X-ray absorption spectroscopy

We carried out an x-ray absorption spectroscopy (XAS) experiment at the Cs L_1, $L_{2,3}$ edges on the microfocus Lucia beamline at SLS (Swiss Light Source, PSI, Villigen) under high pressure up to 14.5 GPa. Further, detailed description of the beamline setup combined with high pressure is fully described in Ref. 50. We worked in the energy range of 5–5.8 keV in the transmission configuration. DAC with stainless steel gaskets and hollowed diamonds were used to minimize x-ray absorption from the environment.[51] The sample was loaded with heavy mineral oil as PTM in a glovebox. Pressure was measured with the ruby fluorescence method. The three x-ray absorption Cs edges were collected using the same setup. In order to reduce the presence of glitches originated from the single crystal diamond anvils, the cell was properly oriented with respect to the x-ray beam.

XAS is a powerful tool for the study of materials under very high-pressure conditions.[52] In particular, it allows to obtain both electronic and structural information of the local environment of atoms (in our case the Cs atoms). The Cs $L_{2,3}$ edges enable the study mainly of d states, whereas in the L_1 edge, p final states are involved, as given by the dipolar selection rules. Information on guest-host hybridization or charge transfer under pressure can be made available through their study. Extended x-ray absorption fine structure (EXAFS) oscillations were obtained for the L_3 edge, allowing, as it will be further discussed, to obtain qualitative in-

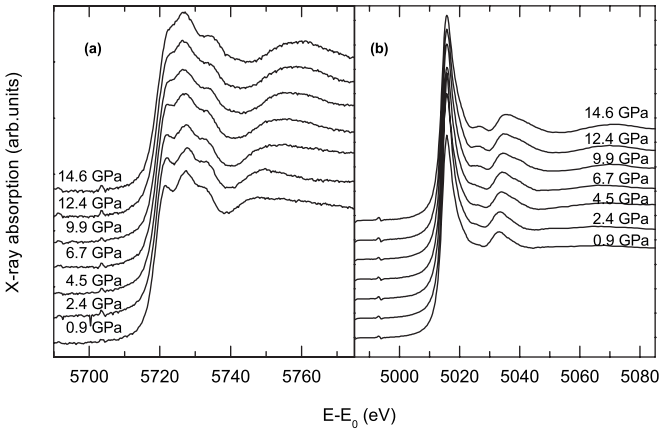

FIG. 13. XANES evolution with pressure at both (a) Cs L_1 edge and (b) Cs L_3 edge of CsC_8 from our experiment at SLS.

formation on the local structure evolution with pressure.

Figure 13 shows the normalized Cs L_1 and L_3 x-ray absorption near edge structure (XANES) evolution as a function of pressure. The L_2 edge is not shown due to a lower signal-to-noise ratio and the similarity with the L_3 edge. For both Cs L_1 and L_3 edges, we observe a progressive evolution of XANES resonances with pressure. No sign of phase transition can be directly derived from the inspection of the XANES evolution. We followed then the inflexion point for the different absorption edges to monitor their energy position as a function of pressure. The absolute error bars in the determination of their energy position were too large to observe a significant evolution in the 0.9–14.5 GPa range. Nevertheless, the accuracy of measurements was high enough to study the pressure dependence of the relative position between the L_1 and L_3 edges at each pressure point. In Fig. 14, we plot the difference of energy position between the L_1 and L_3 edges as a function of pressure. An abrupt jump of approximately 1 eV occurs between 7 and 10 GPa. This sudden change can be related to charge transfer effects between guest Cs atoms and the graphite host. Selection rules impose that this changes concern p states and/or d states. However, there is no further information allowing to establish the relative weight of charge transfer between the p and d channels.

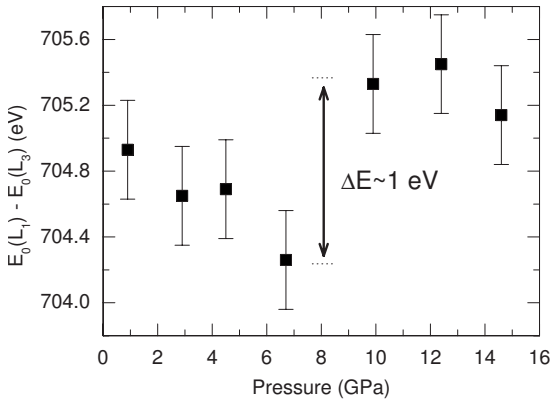

FIG. 14. Difference between the energy of the L_1 and L_3 Cs edges in CsC_8 as a function of pressure.

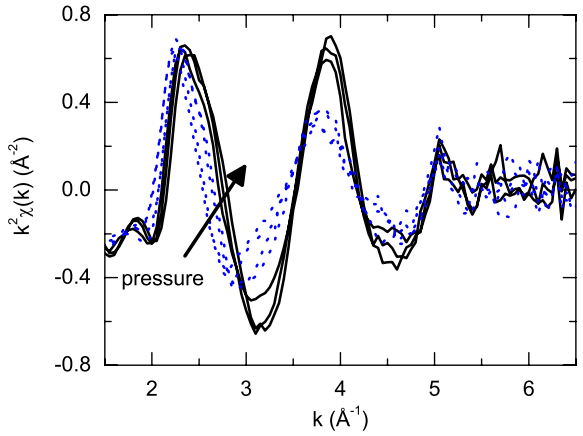

FIG. 15. (Color online) Extracted Cs L_3 edge EXAFS oscillations as a function of pressure. The arrow shows increasing pressures from 0.9 to 14.6 GPa. Dotted lines correspond to the low pressure phase, and continuous lines to the high-pressure phase (see text).

Let us now turn to the EXAFS part of the spectrum. The Cs L_3 edge EXAFS oscillations were extracted from the absorption spectra with the standard AUTOBK procedure.[53] The obtained EXAFS oscillations are shown in Fig. 15, which are expressed in terms of the photoelectron wave number $k = 1/[\hbar\sqrt{2m(E-E_0)}]$, where m is the electron mass and E_0 is the absorption edge position. The limited extent of the signal originates from dynamic or static disorder as well as due to the low-Z values of the main photoelectron scatterers (C atoms). In spite of the reduced k domain, we can appreciate important changes in the amplitude of EXAFS oscillations in the region between 2.5 and 4.5 $Å^{-1}$. These changes correspond to a sudden increase of the amplitude of the signal that takes place between 7 and 10 GPa and that can be associated with the observed changes in the relative position of the x-ray absorption edges (Fig. 14).

Due to the reduced k window for the EXAFS oscillations and the presence of disorder in the material, we have restricted the quantitative analysis to the first shell of carbon neighbors around the absorbing Cs atoms. We used the *ab initio* FEFF 8.0 code[54] (based on Hedin-Lundqvist exchange potential) to generate the scattering functions (amplitude and phase shift of the photoabsorbed and backscattered atoms). The EXAFS oscillations corresponding to the first shell of C atoms around the Cs absorbers were Fourier filtered and fitted with the first single diffusion path using the FEFFIT program.[55] In addition to the Cs-C first neighbor distance [Fig. 16(a)] and the associated pseudo-Debye-Waller factor, we considered also the third cumulant as the only free parameters in our fitted EXAFS expression. We used the cumulant expression implemented in the FEFFIT program based on an anharmonic effective pair potential. The observed change in magnitude of the EXAFS oscillations translates into a modification of the pseudo-Debye-Waller contribution, as shown in Fig. 16(b). The contribution of local disorder effects (thermal or structural) through the C_3 cumulant allows to reproduce the graphite interplane distance, in good agreement with our other data from XRD and NPD (Fig. 17).

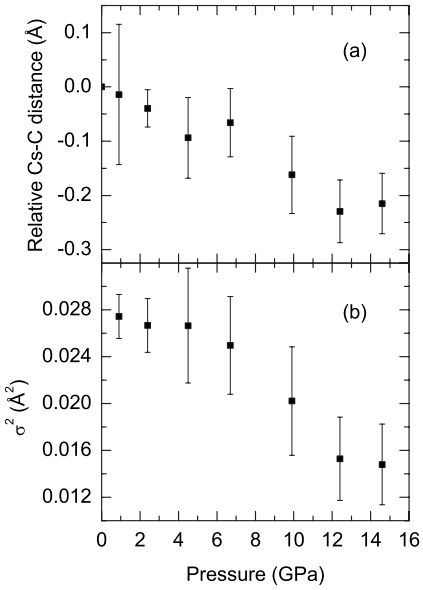

FIG. 16. Pressure evolution of (a) the relative Cs-C first neighbor distance and (b) the pseudo-Debye-Waller σ^2. The EXAFS signal was k^2 weighted and Fourier transformed $[2.5,6.0]$ Å^{-1} to real space and finally fitted in the range $[1,3]$ Å.

III. DISCUSSION

As it is shown in Table IV, we can distinguish four domains of stability of CsC_8. The transitions between these domains are characterized either by modifications in the crystalline structure (as determined by XRD, NPD, or by Raman spectroscopy) or by modifications of the electronic structure (evidenced either by XAS or Raman spectroscopy). The most remarkable facts are the smooth evolution both of the c lattice parameters obtained by NPD up to 9 GPa and of the Cs-C distances given by EXAFS up to 14.6 GPa even if the incertitudes remain very large in this last case. The high sensitivity of XRD to the Cs atom ordering with respect to

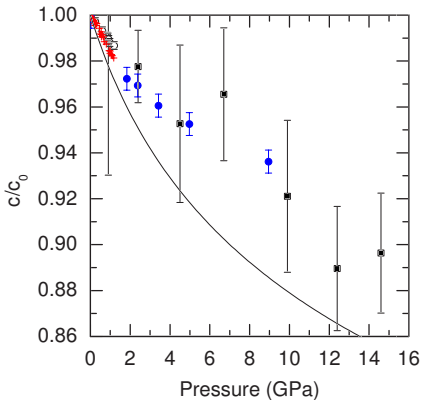

FIG. 17. (Color online) Dependence of the CsC_8 graphitic interplane distance with pressure combining both diffraction (XRD and NPD) data indicated by empty and solid circles and local spectroscopy (EXAFS) data indicated by solid squares. Crosses from 0 to 1.1 GPa correspond to the data of Wada (Ref. 24). The compressibility of graphite (solid line) from Ref. 41 is plotted for comparison.

NPD lets us conclude that the two first phase transitions up to 14.0 GPa are related to slight modifications of the arrangement of Cs atoms, which involve the modification of the correlation between the different layers. In fact, the best fits to the XRD data at 2.0 GPa were performed with a very large unit cell (a=5.24 Å, b=6.02 Å, and c=56.75 Å, SG $C222$, No. 21) which is, in addition, not commensurate with the graphitic subnetwork.

The I→II phase transition is particularly clear, as it is well defined and both observed by XRD and by Raman spectroscopy. The comparison of XRD and NPD data points out a modification of Cs decoration without changes in the graphitic plane stacking because, in spite of their relative intensity changes, (00ℓ) reflections are observed during the whole compression. The important change in the high-frequency Raman peak position at the I→II phase transition could be interpreted as a stage modification. Nevertheless, this appears as contradicting with the NPD data. A possible interpretation is that Raman spectroscopy being more surface sensitive in this metallic compound, staging transitions could be observable at the grain surface. The II→III phase transition, as already discussed, has only been detected through XRD and it may be accompanied by the presence of an intermediate phase. As for phase II, phase III seems to involve a very large crystalline lattice, as suggested by the appearance of low-angle difraction peaks. NPD does not show any difference between phases I, II, and III, so again CsC_8 III is most probably associated with changes in the decoration of the Cs subnetwork. The last phase transition, III→IV at around 8 GPa, is related to changes of the electronic structure, which could imply a stage transition. It is clearly observed by XAS with the associated 1 eV shift between the Cs L_2 and L_3 absorption edges and by Raman spectroscopy with an interior graphitic layer mode and a bounding layer mode, characteristic of a high-stage $n>2$. This transition occurs in all the sample since XAS is a bulk probe. The observation of a doublet in the Raman signal from around 10 GPa is very intriguing, as there are no concomitant observations at this pressure with diffraction techniques. Again, we could invoke the surface sensitivity of Raman spectroscopy in metallic samples to explain this observation. Furthermore, we cannot exclude that this doublet could result from a local laser heating during the experiment. As we do not have NPD data above 9 GPa and fits of the XRD data in this region are not reliable, we cannot assure the persistence of stage 1. Other structural changes associated with the transition around 8 GPa cannot be excluded. Indeed, $n\rightarrow n+1$ staging transition implies the presence of an additional phase to maintain the density of Cs atoms.

Let us now turn to the compressibility of the structure. Compressibility of phase I, characterized either by the volume bulk modulus or by the linear bulk modulus of the c axis, is given in Table II. Our values are compared with other values from the literature which propose higher compressibilities. As mentioned, the neutron diffraction data (Fig. 5) show a smooth variation of the graphiticlike cell parameters with pressure that do not appear to be affected by any clear phase transitions within the calculated incertitude. With a Murnaghan fit up to the highest pressure measured in the NPD experiment, i.e., 8.9 GPa, we obtain a bulk modulus

TABLE IV. Summary of the principal changes observed in the CsC_8 compound as a function of pressure.

	P stability (GPa)	Observed structures	Most significant changes at phase transition and other relevant information
CsC_8 I	0.0–1.2	$P6_222$ stage 1 ($\alpha\beta\gamma$)	Linear compressibility
CsC_8 II	1.2–3.5	$C222$[a]	Change in the Cs decoration accompanied with small displacements and strong modification of the Raman signal
		stage 1+?	Abrupt change in the relative intensity of (003) and (006) diffraction lines, strong broadening of the diffraction lines in NPD
CsC_8 III	3.5–8.0	$Fddd$[a]	Changes in the Cs decoration (slight displacements), in the stacking ($\alpha\beta\gamma\delta$), and possible intermediate structure between II and III
		stage 1+?	Broadening of the diffraction lines in NPD
CsC_8 IV	8.0–32.0	stage n ($n>2$)	Electronic changes observed by EXAFS and Raman at the transition
		+ other phase ?	Significant broadening of the diffraction lines and very low-intensity signal in XRD; no evidence of the presence of stage 1. Doublet observed in the Raman signal

[a]Proposed space groups.

equal to 72 GPa, which, as can be seen in Table II, is closer to the value published by Wada.[24]

In addition, we deduced the graphitic interplane compressibility from the projection of the Cs-C distance on the c axis by EXAFS. Taking into account an anharmonic correction through the third cumulant related to this distance allows to provide a reasonable agreement with the compressibility obtained by the diffraction experiments within the incertitudes (Fig. 17). Introduction of disorder variations in the EXAFS expression to best fit the diffraction data should be a consequence of the changes in the Cs atom decoration observed in the XRD patterns. We observe in Fig. 16(b) from the pseudo-Debye-Waller factor evolution that compression leads to a progressive reduction of the static or/and dynamic disorder of the local Cs structure.

IV. CONCLUDING REMARKS

Combining different techniques, we have studied the pressure behavior of the guest and host subnetworks and the guest-host interaction of the CsC_8 intercalated graphite in the 0–32 GPa range. Three pressure-induced transformations have been clearly observed. The high reactive nature of the sample coupled with its ill order nature made the use of complementary experimental techniques a necessity. The combination of these techniques, in which different selectivities apply, has been essential for the understanding of the observed transitions. We have given evidence of evolution in both the electronic structure (using Raman and XAS spectroscopies) and in the crystallographic structure (XRD and NPD) occurring in the studied pressure range. The main observed facts can be summarized as follows: (i) the anisotropic compressibility with the c axis softer than the in-plane one, (ii) stiffening of the c axis in CsC_8 in comparison with graphite up to 8.9 GPa due to the presence of intercalated Cs atoms (Table II), (iii) subtle rearrangements of the Cs atom layers lead to the observation of complex lattices at high pressure, (iv) a reorganization of the stacking probably occurs (from hexagonal $\alpha\beta\gamma$ to orthorhombic $\alpha\beta\gamma\delta$ at 4.8 GPa, for example), and (v) hybridization between Cs atoms and graphite layers could explain the charge transfer observed in XAS around 8 GPa. Finally, with the exception of the appearance of an impurity phase, it seems that these transformations are reversible at least up to ~8 GPa, indicating that they do not result from a deintercalation process.

ACKNOWLEDGMENTS

This work was supported by the French Ministère Délégué la Recherche et aux Nouvelles Technologies and the CNRS through Grants No. "ACI-2003 n. NR0122" and No. "ACI-2003 n. JC2077." We gratefully thank H. Feret (LPMCN, France) for his assistance and technical support. This research project has been supported by the European Commission under the 6th Framework Programme through the Key Action: Strengthening the European Research Area, Research Infrastructures (Contract No. RII3-CT-2004-506008). Part of this work is based on experiments performed at the European Synchrotron Radiation Facility and at the Swiss Spallation Neutron Source SINQ, Paul Scherrer Institute, Villigen, Switzerland.

*Corresponding author. alfonso.san.miguel@lpmcn.univ-lyon1.fr

[1] M. S. Dresselhaus and G. Dresselhaus, Adv. Phys. **51**, 1 (2002).
[2] T. E. Weller, M. Ellerby, S. S. Saxena, R. P. Smith, and N. T. Skipper, Nat. Phys. **1**, 39 (2005).
[3] N. Emery, C. Herold, M. d'Astuto, V. Garcia, C. Bellin, J. F. Mareche, P. Lagrange, and G. Loupias, Phys. Rev. Lett. **95**, 087003 (2005).
[4] J. S. Kim, R. K. Kremer, L. Boeri, and F. S. Razavi, Phys. Rev. Lett. **96**, 217002 (2006).
[5] G. Lamura, M. Aurino, G. Cifariello, E. Di Gennaro, A. Andreone, N. Emery, C. Hérold, J.-F. Marêché, and P. Lagrange, Phys. Rev. Lett. **96**, 107008 (2006).
[6] N. Bergeal, V. Dubost, Y. Noat, W. Sacks, D. Roditchev, N. Emery, C. Hrold, J.-F. Mareche, P. Lagrange, and G. Loupias, Phys. Rev. Lett. **97**, 077003 (2006).
[7] M. Sutherland, N. Doiron-Leyraud, L. Taillefer, T. Weller, M. Ellerby, and S. S. Saxena, Phys. Rev. Lett. **98**, 067003 (2007).
[8] D. G. Hinks, D. Rosenmann, H. Claus, M. S. Bailey, and J. D. Jorgensen, Phys. Rev. B **75**, 014509 (2007).
[9] R. Cubitt, J. S. White, M. Laver, M. R. Eskildsen, C. D. Dewhurst, D. McK. Paul, A. J. Crichton, M. Ellerby, C. Howard, Z. Kurban, and F. Norris, Phys. Rev. B **75**, 140516(R) (2007).
[10] M. Calandra and F. Mauri, Phys. Rev. Lett. **95**, 237002 (2005).
[11] G. Csanyi, P. B. Littlewood, A. H. Nevidomskyy, C. J. Pickard, and B. D. Simons, Nat. Phys. **1**, 42 (2005).
[12] I. I. Mazin, Phys. Rev. Lett. **95**, 227001 (2005).
[13] M. Calandra and F. Mauri, Phys. Rev. B **74**, 094507 (2006).
[14] I. I. Mazin, L. Boeri, O. V. Dolgov, A. A. Golubov, G. B. Bachelet, M. Giantomassi, and O. K. Andersen, Proceedings of the MZS Conference, Dresden, 2006 [Physica C **460**, 116 (2007)].
[15] A. Sanna, G. Profeta, A. Floris, A. Marini, E. K. U. Gross, and S. Massidda, Phys. Rev. B **75**, 020511(R) (2007).
[16] A. San-Miguel and P. Toulemonde, High Press. Res. **25**, 159 (2005).
[17] D. Connétable *et al.*, Phys. Rev. Lett. **91**, 247001 (2003).
[18] X. Blase, P. Gillet, A. San Miguel, and P. Mélinon, Phys. Rev. Lett. **92**, 215505 (2004).
[19] G. Parry, Mater. Sci. Eng. **31**, 99 (1977).
[20] F. Rousseaux, R. Moret, D. Guerard, and P. Lagrange, Phys. Rev. B **42**, 725 (1990).
[21] C. D. Fuerst, J. E. Fischer, J. D. Axe, J. B. Hastings, and D. B. Mc Whan, Phys. Rev. Lett. **50**, 357 (1983).
[22] J. M. Bloch, H. Katz, D. Moses, V. B. Cajipe, and J. E. Fischer, Phys. Rev. B **31**, 6785 (1985).
[23] C. D. Fuerst, D. Moses, and J. E. Fischer, Phys. Rev. B **24**, 7471 (1981).
[24] N. Wada, Phys. Rev. B **24**, 1065 (1981).
[25] A. Gauzzi, S. Takashima, N. Takeshita, C. Terakura, H. Takagi, N. Emery, C. Herold, P. Lagrange, and G. Loupias, Phys. Rev. Lett. **98**, 067002 (2007).
[26] R. P. Smith, A. Kusmartseva, Y. T. C. Ko, S. S. Saxena, A. Akrap, L. Forró, M. Laad, T. E. Weller, M. Ellerby, and N. T. Skipper, Phys. Rev. B **74**, 024505 (2006).
[27] R. Clarke, N. Wada, and S. A. Solin, Phys. Rev. Lett. **44**, 1616 (1980).
[28] S. Los, M. Letellier, P. Azais, and L. Duclaux, J. Phys. Chem. Solids **67**, 1182 (2006).
[29] J. Rodriguez-Carvajal, Physica B **192**, 55 (1993).
[30] D. Guérard, P. Lagrange, M. ElMakrini, and A. Herold, Carbon **16**, 285 (1978).
[31] A. P. Hammersley, S. O. Svensson, M. Hanfland, A. N. Fitch, and D. Hausermann, High Press. Res. **14**, 235 (1996).
[32] H. K. Mao, P. M. Bell, J. W. Shaner, and D. J. Steinberg, J. Appl. Phys. **49**, 3276 (1978).
[33] P. Fischer *et al.*, Physica B **276**, 146 (2000).
[34] S. Klotz, G. Hamel, and J. Frelat, High Press. Res. **24**, 219 (2004).
[35] S. Klotz, T. Strassle, G. Rousse, G. Hamel, and V. Pomjakushin, Appl. Phys. Lett. **86**, 031917 (2005).
[36] R. Sherley, *The Crysfire 2002 System for Automatic Powder Indexing: User's Manual* (The Lattice, Guildford, 2002).
[37] J. Laugier and B. Bochu, CHECKCELL, LMGP suite of programs for the interpretation of x-ray experiments, Enspg/Laboratoire des Matériaux et du Génie Physique, Saint Martin d'hères, France, 2004 (http://www.inpg.fr/ and http://www.ccp14.ac.uk/tutorial/lmgp/).
[38] P. Lagrange, D. Guerard, M. ElMakrini, and A. Herold, C. R. Seances Acad. Sci., Ser. C **287**, 179 (1978).
[39] V. A. Nalimova, D. Guerard, D. E. Sklovsky, and D. Cox, J. Phys. Chem. Solids **57**, 771 (1996).
[40] B. H. Toby, J. Appl. Crystallogr. **34**, 210 (2001).
[41] M. Hanfland, H. Beister, and K. Syassen, Phys. Rev. B **39**, 12598 (1989).
[42] H. J. Kim, J. E. Fischer, D. B. McWhan, and J. D. Axe, Phys. Rev. B **33**, 1329 (1986).
[43] T. Yagi, W. Utsumi, M.-a. Yamakata, T. Kikegawa, and O. Shimomura, Phys. Rev. B **46**, 6031 (1992).
[44] R. J. Nemanich, S. A. Solin, and D. Gúerard, Phys. Rev. B **16**, 2965 (1977).
[45] P. C. Eklund, G. Dresselhaus, M. S. Dresselhaus, and J. E. Fischer, Phys. Rev. B **16**, 3330 (1977).
[46] G. L. Doll, P. C. Eklund, and J. E. Fischer, Phys. Rev. B **36**, 4940 (1987).
[47] P. C. Eklund and K. R. Subbaswamy, Phys. Rev. B **20**, 5157 (1979).
[48] N. Caswell and S. A. Solin, Phys. Rev. B **20**, 2551 (1979).
[49] T. L. Schindler and Y. K. Vohra, J. Phys.: Condens. Matter **7**, L637 (1995).
[50] A. M. Flank *et al.*, Nucl. Instrum. Methods Phys. Res. B **246**, 269 (2006).
[51] J. P. Itié, F. Baudelet, A. Congeduti, B. Couzinet, F. Farges, and A. Polian, J. Phys.: Condens. Matter **17**, S883 (2005).
[52] J. P. Itie, A. Polian, D. Martinez, V. Briois, A. DiCicco, A. Filipponi, and A. San Miguel, J. Phys. IV **7**, 31 (1997).
[53] M. Newville, P. Livins, Y. Yacoby, J. J. Rehr, and E. A. Stern, Phys. Rev. B **47**, 14126 (1993).
[54] A. L. Ankudinov, B. Ravel, J. J. Rehr, and S. D. Conradson, Phys. Rev. B **58**, 7565 (1998).
[55] M. Newville, B. Ravel, D. Haskel, J. J. Rehr, E. A. Stern, and Y. Yacoby, Physica B **209**, 154 (1995).
[56] H. Zabel and A. Magerl, Phys. Rev. B **25**, 2463 (1982).
[57] M. Mohr, J. Maultzsch, E. Dobardzic, S. Reich, I. Milosevic, M. Damnjanovic, A. Bosak, M. Krisch, and C. Thomsen, Phys. Rev. B **76**, 035439 (2007).